Internally driven spatiotemporal irregularity in a dc glow discharge

A. Dinklage* and C. Wilke
Institut für Physik, Ernst-Moritz-Arndt-Universität Greifswald, Domstrasse 10a, 17 487 Greifswald, Germany

G. Bonhomme and A. Atipo
Laboratoire de Physique des Milieux Ionisés, ESA 7040 du CNRS, Université Henri Poincaré, Boîte Postale 239, 54 506 Nancy, France
(Received 8 May 2000)

Spatiotemporal dynamics of an undriven dc glow discharge at intermediate pressures ($p_0 r_0 = 6.2$ Torr cm, $i < 50$ mA) is investigated experimentally. Spatiotemporal irregularity and windows of regular nonlinear waves occur and are found to depend on the discharge current. Above a threshold current column head oscillations arise and inject high-frequency ionization waves into the positive column that decay towards the anode through nonlinear wave coupling with a discrete eigenmode of the positive column. Regularity was found to be a result of commensuration of both waves and obeys a devil's staircase. Since column head oscillations occur in the transition region from cathode fall to positive column as result of discharge formation, the irregularities were internally driven. Spatiotemporal analysis by means of biorthogonal decomposition gives insights into the mechanism of irregularity and can be employed for characterization of spatiotemporal complexity.

PACS number(s): 52.35.Py, 52.80.Hc, 05.45.−a

I. INTRODUCTION

Extended dissipative systems far from equilibrium may exhibit complex spatiotemporal dynamics leading to the formation of regular patterns or turbulence [1]. Understanding this dynamics is a challenging problem in modern physics that offers a key for applications of nonlinear systems. Outstanding examples of nonequilibrium pattern formation can be found in discharge plasmas [2–4]. These plasmas are governed by dissipative effects and are far from equilibrium in a double sense. First, the electrical power is dissipated by heat conduction, flow of long-lived excited atoms to the walls and radiation, respectively. Second, the electron gas and the neutral atoms have strongly different distribution functions and, as a rule, the lower the neutral gas pressures, the more the energy distribution of the electrons differs from a Maxwellian. For pressures discussed here the electron temperatures are much higher than the neutral gas temperature [5].

In these discharges, which may be considered as field affected reaction-diffusion systems, the positive column destabilizes owing to the ionization instability [6] leading to light fluctuations. In inert gas discharges, which will be considered subsequently, the discharge current i acts as a control parameter for a given geometry and neutral gas pressure p_0. Variation of i results in different bifurcations. As a rule, for small currents the plasma is homogeneous and all fluctuations are damped. Above a threshold value i_c, a Hopf bifurcation leads to ionization waves [7] that can be classified by the energy the electrons gain along one wavelength, the so-called Novak number [8,9]. These waves disappear when a much higher discharge current, the so-called Pupp limit i_{Pupp} [10], is exceeded. In between these limits ($i_c < i < i_{Pupp}$) sequences of various secondary bifurcations can be observed including mode transitions [11] and transitions from regular to irregular dynamics.

Ionization waves are longitudinal waves propagating along the discharge axis leading to a modulation of the light emerging from the discharge. Dispersion of ionization waves in a neon gas discharge [12] ($\omega \propto k^{-1}$) results in phase velocities opposite to the group velocity. Therefore these striations are called backward waves. The group velocity is directed from cathode to anode, which is the direction of electron flow. The amplitude of the waves grows exponentially from the cathode side of the positive column and becomes saturated towards the anode. Feedback through the external circuit provides longitudinal spatial eigenmodes [13,14] that can be parametrized by an integer mode number n by $k_n = 2\pi L/n$, where L is the length of the discharge.

This phenomenon and the fact that substantial inhomogenities occur close to the cathode dark spaces, may lead to the conclusion that the cathode region is the origin of ionization waves [15]. However, there is much evidence both experimentally [6,16] and theoretically [7,17] that it is the plasma of the positive column that represents an excitable medium that destabilizes owing to *the existence of constraints* (here the external voltage) and *conservation laws* [1] (here current conservation). In addition the real discharge is affected by the external circuit (feedback mechanisms [13]) and by finite length effects leading to transition regions at the anode (e.g., anode spots [2]) and at the cathode (space-charge regions, dark spaces). These features may lead to additional instabilities of the entire discharge that complicate the situation. These effects underline the necessity that for a complete understanding of the discharge plasma both boundaries and the external circuit have to be considered. Thus, the investigation of the entire discharge including the transition regions should be expected to give new insights into discharge physics.

This paper examines the influence of the transition region between the cathode region and the positive column on the ionization instability. This transition region is known as the

*Present address: Max-Planck-Institut für Plasmaphysik, EURATOM Association, Teilinstitut Greifswald, Wendelsteinstrasse 1, 17 491 Greifswald, Germany.

head of the positive column or—briefly—the *column head*. The column head is a distinct bright ball at the cathode side of the positive column whose axial extent is in the order of the lateral dimension, i.e., the tube diameter. Generally, the head is followed by a sequence of spatially damped standing striations settling to the homogeneous positive column. A similar spatial response can be observed when the plasma of the positive column is disturbed by a probe or if a small region of the plasma is irradiated by light tuned to an allowed transition starting from a metastable level [18]. Hence, the column head can be regarded as a spatial relaxation phenomenon of the initial perturbation owing to cathode dark spaces. We note that this transition is a self-organized region of the discharge provided the length of the discharge allows a positive column to be established.

The column head is known to oscillate above a threshold value i_{ch} [19]. The frequency of this oscillation, as will be shown later, is a linearly growing function of discharge current. Experimental evidence demonstrates that these oscillations inject an ionization wave that interacts with the fundamental mode of the positive column. It will be shown that this interaction leads to sequences of regular and irregular spatiotemporal patterns depending on the discharge parameters.

There are some early reports on the spatiotemporal dynamics of the plasma when head oscillations are present [20]. Although it has been suspected that a frequency mismatch leads to irregularity [21], no systematic investigations on the occurrence of irregular patterns are reported.

Regularity of the spatiotemporal patterns is investigated by means of the biorthogonal decomposition [22]. These results lead to an explanation of the irregular spatiotemporal dynamics observed in the positive column. Since the column head is self-organized, spatiotemporal patterns formed in the positive column are said to be internally driven.

II. EXPERIMENTAL RESULTS

Experiments were performed in a sealed cylindrical Pyrex glass tube (internal radius $r_0 = 2.0$ cm) which was filled with spectroscopically pure neon ($p_0 = 3.168$ Torr at 273 K). Considerable attention was paid to prevent impurities in the tube including thorough baking of the tubes and eddy current heating of the electrodes during preparation of the tubes. Figure 1 shows a schematic representation of the experimental setup. The tube consisted of a hollow cathode and a plane anode machined from molybdenum. The anode-cathode spacing was $L = 68$ cm. The discharge was sustained by a high-voltage supply. Discharge current was limited by a load ($R = 50$ kΩ). Since the waves lead to a modulation of the light emerging from the discharge, a fast (CCD) camera (256 pixels, line frequency <33 kHz, typical frequency of the waves <2 kHz) was employed for detection of the spatiotemporal dynamics of the waves.

As the dynamics was of particular interest, the occurrence of the different wave states was examined first. For this purpose spectra of the light fluctuation were taken below $i < 50$ mA for all operating currents. Spectra were detected by means of a photodiode and a (fast Fourier transform) spectrum analyzer. The photodiode was positioned close to the anode because the amplitude of the light fluctuations was

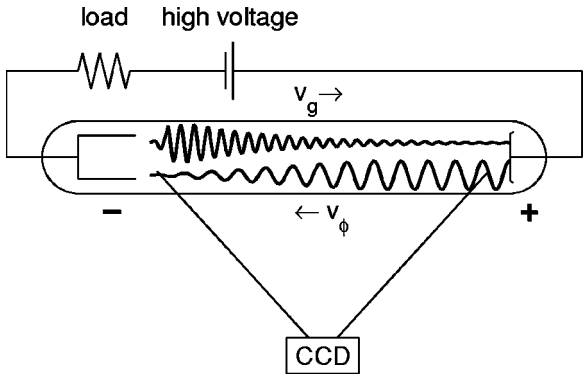

FIG. 1. Schematic diagram of the experimental setup and essential detection devices. The spatial development of the high-frequency wave and the eigenmode of the positive column are indicated by the spatial oscillations in the discharge tube. v_g indicates the direction of the group velocity and v_Φ the direction of the phase velocity.

largest at this position, which is important for low-discharge currents, i.e., no saturation of the wave amplitudes occurs. Figure 2 shows the power spectral density of light fluctuation close to the anode. Here we restrict ourselves to the most relevant frequencies below $f < 6.25$ kHz. Whiteness represents the power spectral density as indicated.

Below $i < 1.1$ mA (white region in Fig. 2) the discharge could not be operated with the load employed here according to Kaufmann's stability criterion [23]. Above this current striations can be observed, indicated by the power spectral

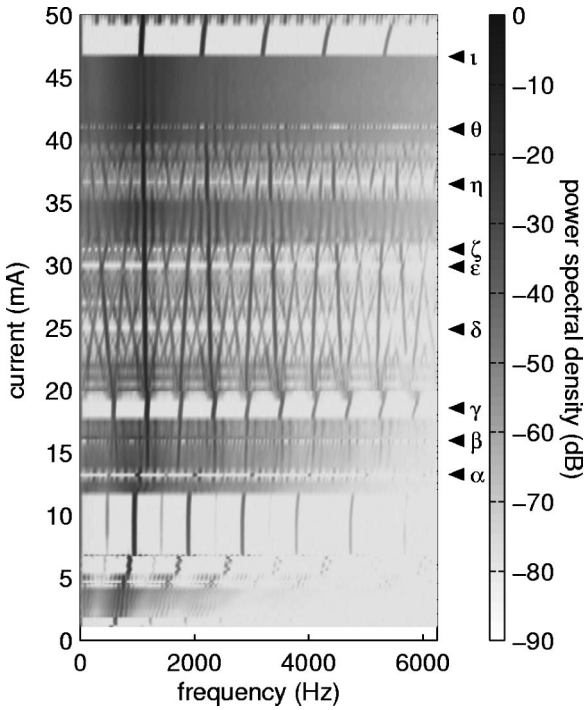

FIG. 2. Power spectral density of light fluctuations taken 1 cm in front of the anode of a neon dc glow discharge (neutral gas pressure $p_0 = 3.168$ Torr at 273 K, internal radius $r_0 = 2.0$ cm). Spectra in the operation regime 1.1 mA$< i <$ 50 mA are displayed. Below $i < 1.1$ mA (white region) the discharge could not be operated. Dark lines correspond to coherent wave modes. Triangles on the right-hand side (greek labels) indicate occurrence of regular waves in the presence of column head oscillations.

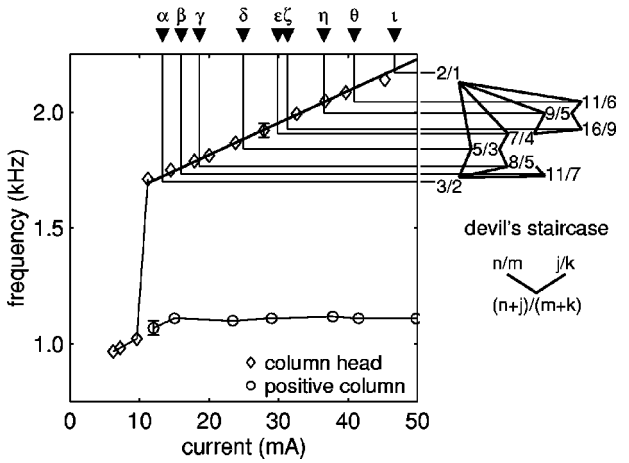

FIG. 3. Dependence of frequencies of maximum power spectral density of light fluctuations emitted from the head (◇) and the near anode region (○) of the positive column on the discharge current. Triangles indicate occurrence of regular wave dynamics. Corresponding frequency ratios are indicated on the right of the diagram. Ratios occurring represent a clipping of a devil's staircase that is formed as shown below the frequency ratios.

density (dark lines in Fig. 2). For currents below $i < 10.6\,\mathrm{mA}$ sequences of highly coherent longitudinal eigenmodes, regions of competing modes, and the occurrence of subharmonics can be observed. A detailed analysis of this behavior is not the subject of this paper.

Here we focus on the region above $i > 10.6\,\mathrm{mA}$ when cathode head oscillations arise. Up to the maximum current investigated ($i_{\max} = 50\,\mathrm{mA}$) complicated spectral structures are observable when the current is increased. However, regular structures as indicated by the triangles on the right side of Fig. 2 can be observed in certain windows of the discharge current. In Fig. 2 these windows are indicated by Greek letters. As a criterion for regularity, distinct peaks in the power spectral density are considered. Irregularity corresponds to broad spectra, which can be identified in Fig. 2 as smeared gray regions. It should be noted that the frequency of the maximum power spectral density in Fig. 2 (close to the anode) remains nearly fixed at about $f_c = 1.1\,\mathrm{kHz}$.

The occurrence of regular windows can be explained by examining both the frequency of column head oscillations and the eigenfrequency of the positive column in detail. Figure 3 shows the current dependence of both frequencies. On the one hand, as already noted, the frequency close to the anode remains nearly fixed. This observation is in accordance with the fact that close to the anode an ionization wave eigenmode is governing the dynamics. The explanation is as follows: Since the electric field in the positive column does not change significantly for larger currents [5], the amplification properties of the plasma do not change significantly either. Additionally, certain eigenmodes are preferred owing to feedback effects. As a result, the most unstable wave mode frequency changes slowly for large currents. On the other hand, the frequency of the current head oscillations obviously increases with the discharge current. An explanation for this observation cannot be given. Consequently, the frequency ratio of the most unstable mode in the positive column f_c and the frequency of the column head f_h is current dependent. Within the experimental errors the occurrence of

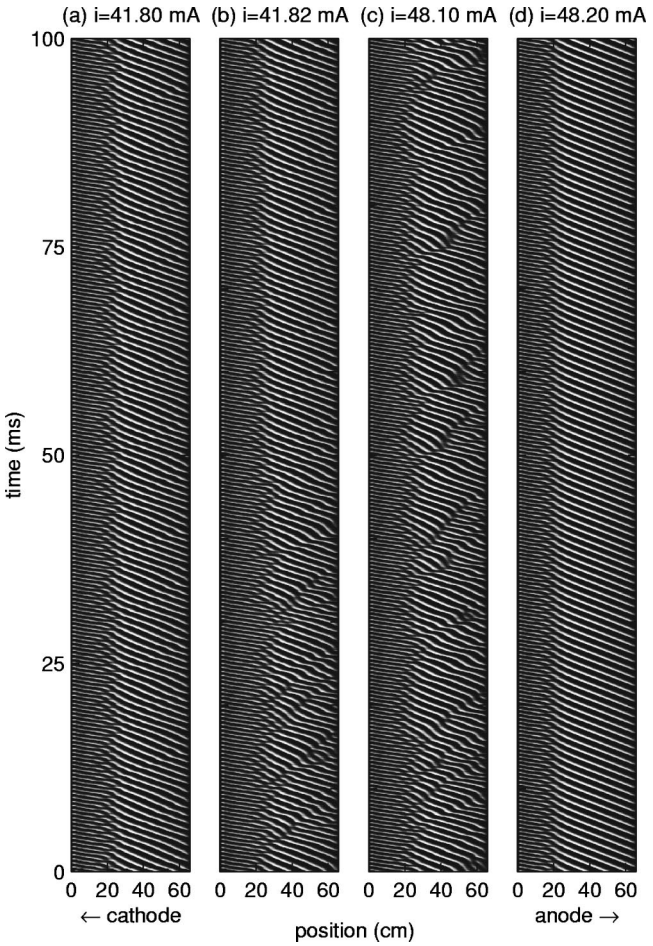

FIG. 4. Spatiotemporal dynamics (films) of light fluctuations owing to ionization waves in a neon dc glow discharge ($r = 2$ cm, $p = 3.1$ Torr). (a) A weakly chaotic state ($i = 41.80$ mA), (b) intermittency between weakly and strongly chaotic states ($i = 41.82$ mA), (c) developed amplitude turbulence ($i = 48.10$ mA) and (d) a regular state ($i = 48.20$ mA). Observations cover the entire positive column including the column head ($x \approx 0$ cm).

regular dynamics is related to a rational ratio of f_h/f_c. Evaluation of these ratios shows that they form part of a devil's staircase which is also typical for the occurrence of regular windows in a driven nonlinear oscillator. This observation is a first hint for the fact that the column head drives the positive column.

This is corroborated by films of the spatiotemporal dynamics of the light fluctuations. Figure 4 shows one-dimensional films (space-time plots) of the light emission emitted from the entire discharge. We chose four situations for larger currents (between labels θ and ι in Fig. 2) in order to examine the spatiotemporal dynamics in a representative way. The following is a discussion of the spatiotemporal dynamics of ionization waves for discharge currents $i = 48.20\,\mathrm{mA}$, $i = 48.10\,\mathrm{mA}$, $i = 41.82\,\mathrm{mA}$, and $i = 41.80\,\mathrm{mA}$, respectively. All spatiotemporal data presented in this paper refer to the visible part of the discharge investigated covering a length of 65.7 cm in front of the anode. The cathode side of the films and all subsequent data is at $x = 0$ cm. For the largest current shown in Fig. 4(d) ($i = 48.20\,\mathrm{mA}$) regular spatiotemporal dynamics is observed. The high-frequency oscillation can be clearly perceived on the cathode side of the discharge ($x \to 0$ cm). This oscillation is the origin of a high-

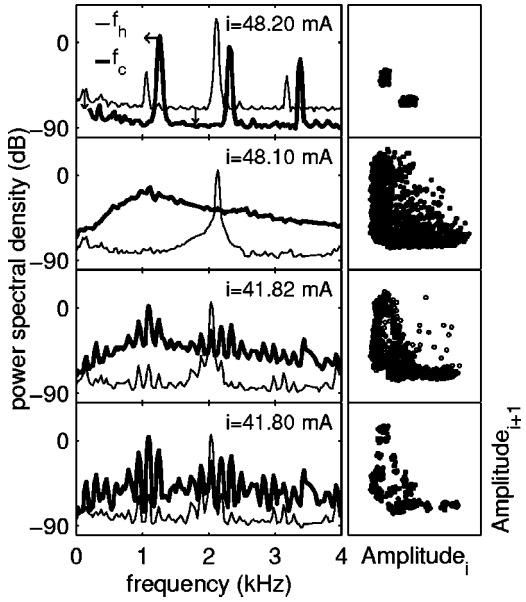

FIG. 5. Left panels show power spectral densities of light fluctuations at fixed positions corresponding to the currents of the films shown in Fig. 4. The fat line corresponds to the dynamics 1 cm in front of the anode. The thin line shows the spectrum of light fluctuations emerging from the column head. For clarity the spectra for $i=48.20\,\mathrm{mA}$ are shifted in power spectral density (f_h) and frequency (f_c) as indicated by the arrows. Right panels show the first return maps to the Poincaré sections of the near anode time series.

frequency wave at large phase velocities. At a very distinct borderline ($x\approx 23\,\mathrm{cm}$) the high-frequency wave merges to a low-frequency one. Then, for positions towards the anode, the positive column exhibits a very regular ionization wave. This film is proof of the statement above, i.e., the column head drives the positive column. For smaller currents shown in Figs. 4(a)–4(c) the spatiotemporal dynamics in the positive column becomes more complicated and will be discussed in the following in more detail. As can be seen from these examples (cf. Fig. 4) spatiotemporal complexity is reflected by the phases of the waves and—for more complex patterns—by the occurrence of spatiotemporal defects. These dislocations represent localized sources and drains for wave crests. As can be seen in Fig. 4(c) dislocations appear at the edge of fronts that propagate through the plasma from cathode to anode. This is the direction of group velocity of ionization waves. But the velocity of the fronts differs strongly from pulse to pulse and depends on the amplitude of the pulse. Dislocations with large amplitude fronts may also occur intermittently as was found for $i=41.82\,\mathrm{mA}$ [cf. Fig. 4(b)]. For this current long intervals of more regular dynamics are found (about 80% of the entire film). Intervals of irregular fronts are comparatively short. The time interval displayed in Fig. 4 was chosen in order to show the transition from irregular to more regular motion. The seemingly regular motion displayed in Fig. 4(a) ($i=41.80\,\mathrm{mA}$) corresponds to weak chaos as will be discussed later.

These observations can be explained if we consider some aspects of the temporal dynamics. The left panels of Fig. 5 shows spectra of time series taken from the data shown in Fig. 4. Corresponding first return maps to Poincaré sections are shown in the right panels. Nyquist frequency is $f_N=12.5\,\mathrm{kHz}$ for all the spectra, but our discussion is restricted to frequencies below 4 kHz. For comparison, spectra from both the column head (thin line, left panels of Fig. 5) and close to the anode are shown (thick line, left panels of Fig. 5). Again, as can be seen from the spectra, each spectrum has a distinct maximum.

First, the column head oscillation spectra (thin lines in Fig. 5) are discussed. The maximum of light fluctuations of column head oscillations is always a distinct peak. As can be seen from comparing of all currents the maximum slightly increases with increasing discharge current. For spatiotemporal irregularity ($i=48.10\,\mathrm{mA}$) all frequencies apart from the maximum are strongly damped. For the regular case, however ($i=48.20\,\mathrm{mA}$) an $f/2$ subharmonic occurs. In addition to subharmonic contributions, sidebands arise for the lower currents ($i=41.82\,\mathrm{mA}$ and $i=41.80\,\mathrm{mA}$).

Second, the spectra of light fluctuations emerging from the positive column close to the anode (thick lines in Fig. 5) are discussed. For regular patterns ($i=48.20\,\mathrm{mA}$) there is a governing peak and higher harmonics due to the pulselike form of the waves. The second harmonic of the fundamental frequency of the light from the positive column matches exactly the driving frequency from the column head. Further coupling is given by higher harmonics not displayed in this graph. For developed irregularity ($i=48.10\,\mathrm{mA}$) the spectrum from the positive column does not exhibit peaklike structures but shows a maximum at the positive column frequency and then diminishes obeying a power law for higher frequencies. For $i=41.80\,\mathrm{mA}$ strong side-band contribution can be identified and sidebands of higher harmonics match with the column head frequency. For slightly higher currents $i=41.82\,\mathrm{mA}$, the structure of the positive column spectrum is very similar except that the underground is strongly lifted. For this case it should be noted that the spectrum was taken for a time series including intermittent bursts. Hence, the spectrum represents an average of time intervals with dynamics similar to the case displayed below ($i=41.80\,\mathrm{mA}$) and above ($i=48.10\,\mathrm{mA}$). This is confirmed by a separate analysis of time intervals with and without fronts and dislocations.

The occurrence of structures in the column head spectrum depends on the power-spectral density maximum of positive column oscillation. If this maximum exceeds a threshold of -5 dB, significant peaks arise from the noise level at -90 dB. Typical damping at the positive column frequency ($f_c=1.1\,\mathrm{kHz}$) can be derived from these data and are found to be -60 dB. These observations support the role of feedback for the formation of striations.

Third, the dynamics is characterized by first return maps to Poincaré sections (Fig. 5, right panels). For this purpose the time series of light fluctuation near the anode was resampled at the maxima of the time series near the cathode. This gives a triggered time series represented by a sequence of amplitude values x_i. A two-dimensional first return map to the Poincaré section can be constructed from the delay plot x_i, x_{i+1}. For regular motion the first return map to the Poincáre section is given by two spots owing to the fact that $f_h/f_c=2$. The width of the spots indicates the experimental error of the procedure applied here. For developed irregularity ($i=48.10\,\mathrm{mA}$) the first return map to the Poincaré section fills a region in the x_i, x_{i+1} plane indicating temporal chaos.

For lower currents it is difficult to examine the dynamics from these first return maps to the Poincaré sections.

For clarity the case $i=41.80\,\mathrm{mA}$ is discussed first. The length of the time series available and the experimental scattering do not allow us to decide whether this section corresponds to a high-dimensional torus (quasiperiodicity), or whether small regions are filled (weak chaos) or if there are distinct spots (periodicity). The first return map to the Poincaré section for $i=41.82\,\mathrm{mA}$ helps to resolve this question. Filled symbols in this plot correspond to time intervals with more regular dynamics and open symbols refer to irregular time intervals. In this case the filled symbols tend to fill out either a certain region in the first return map to the Poincaré section or to form a section through a torus. Hence, periodic dynamics can be excluded. It is interesting to note that during intermittent occurrence of bursts the open symbols may strongly depart from the limited region formed by the filled symbols. A characterization of time series corresponding to the spectrum Fig. 5 ($i=41.80\,\mathrm{mA}$) by correlation dimensions and estimating Lyapunov exponents [24] failed. However, the Kolmogorov entropy could be estimated [25] yielding a value of $H_K=0.3\pm0.1$. This indicates that the underlying time series of the spectrum in Fig. 5 ($i=41.80\,\mathrm{mA}$) is weakly chaotic. Hence, the case $i=41.82\,\mathrm{mA}$ can be regarded as an example of intermittence between weak spatiotemporal chaos as shown in Fig. 4(a) and amplitude defect turbulence as displayed in Fig. 4(c).

In order to examine both the underlying wave physics and the spatiotemporal complexity the space-time diagrams were analyzed by means of the biorthogonal decomposition.

III. BIORTHOGONAL ANALYSIS OF SPATIOTEMPORAL PATTERNS

Space-time characterization of spatiotemporal irregularity is a poorly understood issue [1,26] and is the subject of current efforts. The method of birothogonal decomposition (BD), also known as Karhunen-Loéve or proper orthogonal decomposition, is A classical statistical tool for characterizing spatiotemporal data [27] or for modeling spatiotemporal systems [28]; for an overview see Refs. [22,29]. The BD is employed for characterization of the spatiotemporal regularity of our experimental results and to analyze the wave dynamics.

The main purpose of this decomposition is to decompose a signal $u(t,x)$ into a minimum number of eigenfunctions in space [topos $\phi_k(x)$] and time [chronos $\psi_k(t)$]. The relevance of these eigenfunctions is reflected by their weights s_k. We restrict ourselves to bias-free, discrete, one-dimensional signals, i.e., the signal may be represented by a matrix $u(t_i,x_j)=U_{ij}$. Then the decomposition reads like

$$U_{ij}=\sum_{k=1}^{K}\psi_k(t_i)\,s_k\,\phi_k(x_j) \tag{1}$$

with

$$i=1,\ldots,N,\quad j=1,\ldots,M\quad\text{and}\quad K=\min(N,M).$$

The chronos and topos represent a least-square optimized real orthonormal basis of the N- and M-dimensional finite spaces of space (length L) and time (length T) observation, respectively. Both chronos and topos fulfil an orthonormality relation (δ_{ij}: Kronecker delta):

$$\int_T \psi_r\psi_s\,dt=\int_L \phi_r\phi_s\,dx=\delta_{ij}\,. \tag{2}$$

The weights of the expansion terms are the eigenvalues of the positive semidefinite covariance matrix $U\,U^T$ ordered in decreasing size.

The method of BD is superior to other multivariate methods since the spatial and the temporal eigenfunctions are treated simultaneously as they are constrained by an isomorphism between the chronos and topos [29]. This makes the BD a powerful tool for the detection of spatiotemporal coherences that are indicated by degenerated modes, i.e., doublets $\psi_k\,s_k\,\phi_k$ with the same weight s_k. In particular, the distribution of the weights is a measure for the spatiotemporal complexity.

Numerical implementation of the BD analysis can be performed by a singular value decomposition of the data matrix.

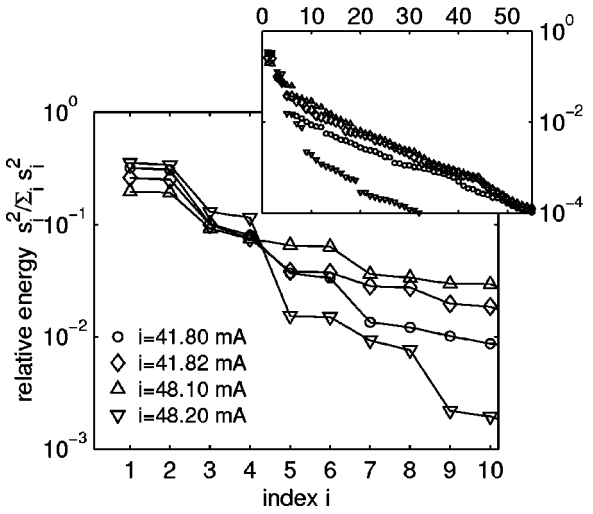

FIG. 6. Relative energy captured by BD modes of index i of the films shown in Fig. 4. Doublets indicate spatiotemporal symmetries. The inset displays the scaling of contribution of higher BD modes.

A. Spatiotemporal complexity

Figure 6 shows the normalized energy content $s_i^2/\Sigma_j s_j^2$ derived from a BD analysis of the data shown in Fig. 4. We have displayed the relative energy in order to compare the four cases that have different absolute variances. As argued above, doublets at small index numbers indicate spatiotemporal coherences. Practically, the eigenfunctions of these degenerated doublets are shifted in phase only and have to be treated as one spatiotemporal mode, the so called BD mode. The results displayed in Fig. 6 show that the first eight weights represents four doublets ($i=1,2$, $i=3,4$, $i=5,6$, and $i=7,8$, respectively) for all cases. For all cases the first doublet ($i=1,2$) governs the spatiotemporal dynamics. Then the second BD mode ($i=3,4$) has approximately the same relative energy content for all currents. Largest deviations in the relative energy content occur in the third BD mode ($i=5,6$). For higher indices complexity can be derived from

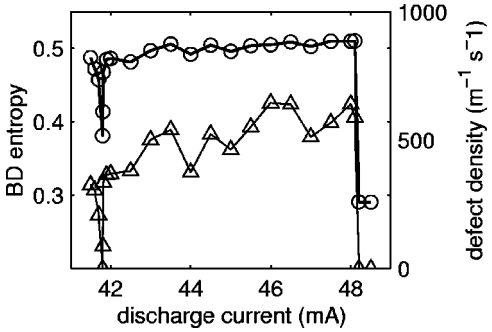

FIG. 7. Measures of spatiotemporal complexity for discharge currents between $i=41.78$ mA and $i=48.50$ mA. ○ correspond to the BD entropy and △ to defect density in the positive column, respectively.

the scaling of the weights as displayed in the inset of Fig. 6. And the larger the high-index weights, the more complex is the spatiotemporal pattern. Since the relative energy $p_k = s_k^2/\Sigma_j s_j^2$ is normalized, an entropy measure can be introduced:

$$H_{BD} = -\frac{1}{\ln K}\sum_{k=1}^{K} p_k \ln(p_k). \tag{3}$$

For the largest complexity possible, all p_k have the same value and the BD entropy becomes maximum $H_{BD}^{max}=1$. The most regular case corresponds to $p_1=1$ and $p_{k>1}=0$ leading to a minimum BD entropy of $H_{BD}^{min}=0$. For the most regular Hopf pattern we have $p_1=p_2=0.5$ and the minimum BD entropy is given by $H_{BD}^{min}=-\ln(0.5)/\ln(K)$. Hence, in practical cases, the minimum BD entropy depends on the resolution of the data matrix either in space or in time. In our case the resolution is given by $K=217$ detector positions and yields $H_{BD}^{min}=0.129$.

Figure 7 shows the dependence of BD entropy on the discharge current for $i>41.78$ mA and $i<48.50$ mA. For these currents, a distinct minimum appears at $i=41.80$ mA [cf. Fig. 4(a)]. Then the BD entropy settles to a high plateau at currents above $i=41.82$ mA, [Fig. 4(b)] and is slightly increasing for currents up to $i=48.1$ mA [Fig. 4(c)] before sharply decreasing when the system becomes regular [$i=48.20$ mA, Fig. 4(d)]. The coarse development of BD entropy reflects the visual inspection of the films as discussed above. Another method for measurements of spatiotemporal complexity is also shown in Fig. 7, where the second plot displays the defect density derived from the spatiotemporal data, which is the number of amplitude defects normalized to the spatial and temporal extent of the films. As amplitude defects all open phases (dislocations) within the films were counted, except for the transition region from high- to low-frequency region ($x\approx 23$ cm). The defect density vanishes for $i=48.20$ mA [Fig. 4(d)] as well as for $i=41.80$ mA [Fig. 4(a)]. It is interesting to note that a fine structure in the plateau ($41.82\text{ mA}<i<48.20\text{ mA}$) appears. These dips cannot be explained by experimental or evaluation errors and seem to be significant. Detailed examination of the current dependence of the BD entropy shows small dips as well.

In order to compare films for different control parameters, both the BD entropy and the defect density seem to be appropriate tools to characterize spatiotemporal complexity. Defect density seems to be more sensitive to detect different stages of defect turbulence. But BD entropy detects also weakly irregular spatiotemporal patterns as can be seen by comparison of the absolute value of BD entropy at $i=41.80$ mA [$H_{BD}(i=41.80\text{ mA})=0.38$] and at $i=48.20$ mA [$H_{BD}(i=48.20\text{ mA})=0.29$]. Both values are less than typical values in the plateau ($H_{BD}\approx 0.5$) indicating more regular dynamics than for developed irregularity. But the absolute value cannot be used as a criterion for the characterization of the spatiotemporal dynamics, i.e., a BD entropy of $H_{BD}=0.5$ does not necessarily indicate defect turbulence. On the other hand, defect density measurements cannot distinguish between weak chaotic and periodic dynamics. But this measure clearly indicates the occurrence of amplitude defects. As a conclusion it is useful to employ different measures for spatiotemporal complexity simultaneously. For details on different stages of spatiotemporal complexity see Ref. [30].

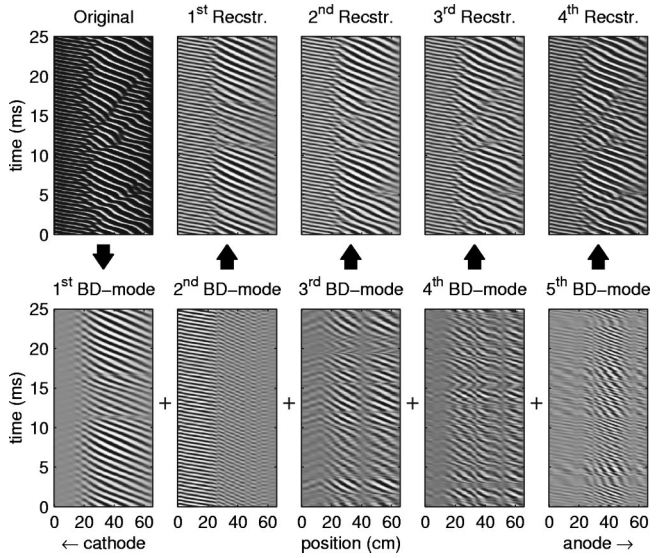

FIG. 8. BD analysis of a 25 ms film for a discharge current of $i=48.10$ mA. The lower row shows films of BD modes, i.e., the superposition of chronos and topos of the doublets occurring in Fig. 4 of the original film (first film in the upper row). The jth reconstruction displayed in the upper row is the superposition of the $j+1$ BD modes.

B. Analysis of mode interaction

Besides the discussion of spatiotemporal complexity the physical relevance of the eigenfunctions should be considered. In the bottom row of Fig. 8 the BD modes for the first 25 ms of the film shown in Fig. 4(c) are displayed. The original data are shown in the left panel of the upper row in Fig. 8. It is useful to discuss these films in conjunction with Fig. 9 where the mean value normalized variance of these films as a function of axis position is displayed. These functions indicate positions of wave activity for any particular mode. For instance, the large oscillation amplitude of the column head can be identified as a peak at position $x\approx 1$ cm in the upper panel of Fig. 9. Additionally, from this figure, the region $x<23$ cm exhibits a smaller amplitude, but the amplitude increases towards the anode and becomes satu-

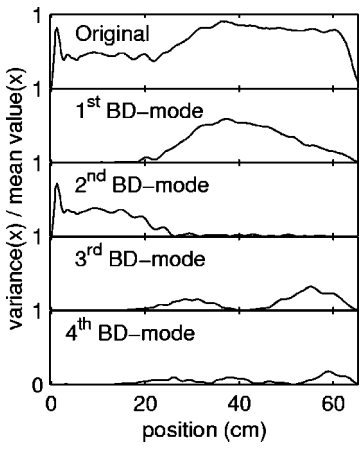

FIG. 9. Spatial development of wave activity for the signal (original; upper panel) and the BD modes as shown in Fig. 8.

rated at positions of about $x \approx 35$ cm. Wave activity decreases near the anode ($61\,\text{cm} < x < 65\,\text{cm}$). As can be seen from the second panel in Fig. 9 wave activity of the first BD mode vanishes for $x < 23$ cm. The second BD mode (third panel in Fig. 9) contains nearly the entire wave activity for $x < 23$ cm if compared to the original data. In particular, the column head oscillation is included in this mode. The space-time diagrams of these BD modes (cf. lower row in Fig. 8) show that these modes represent a more or less regular mode, which is active in the positive column only (first BD mode). The second BD mode is the high-frequency wave injected from the column head oscillation. It should be noted that this film is extraordinarily regular. But, as can be clearly seen from Fig. 9, this mode disappears towards the anode. Instead, wave activity of higher BD modes becomes more relevant in this positive column region ($x > 23$ cm). Detailed analysis of wavelength and frequency of any particular modes show that the dispersion of these waves is consistent with dispersion properties of real ionization waves. Moreover, higher BD modes can be assigned to different longitudinal eigenmodes. As can be seen in Fig. 8, these higher BD modes appear transiently. In particular for time intervals when the first BD mode appears to be blurry, these modes become active.

Physical relevance of these transiently occurring modes can be derived from the low-order reconstructions, i.e., the weighted superposition of the BD modes. These reconstructions are shown in the upper row of Fig. 8. The first reconstruction, which is the superposition of the eigenmode of the positive column (first BD mode) and the high-frequency column head wave (second BD mode) already reconstructs some major features of the original film, i.e., two spatially interacting wave modes. Additionally, it can be clearly seen from this reconstruction that the apparent spatiotemporal defects at the transition border $x \approx 23$ cm are results of wave superposition. We would like to remark that similar structures were already noted by the Belfast group [20]. They concluded, as interconnecting the heads of each apparent defect leads to an opposite phase velocity than that of ordinary ionization waves, that these patterns correspond to forward waves. Our analysis confirms the existence of forward modes, as can be seen from the near cathode region of the third BD mode (cf. Fig. 8). It is interesting to note that the forward mode seems to arise from a region at $x \approx 12$ cm. In this region the phases of forward and backward waves match.

By adding more BD modes to the reconstructed film, more details appear. In particular, defects and fronts appear. By comparison of the original film and the reconstruction the relevance of the transiently occurring modes becomes clear. These modes are active when fronts and spatiotemporal defects appear. Since wavelengths and frequencies of these modes correspond to longitudinal eigenmodes of the plasma the appearance of defects and fronts has to be interpreted as the result of transient multimode interaction. This can be interpreted as the reaction of the system to the necessity of energy transfer from the high-frequency wave to the low-frequency, most unstable, wave mode.

This example shows that results of the BD analysis may yield physically relevant eigenfunctions.

IV. SUMMARY

The spatiotemporal dynamics of an undriven dc neon glow discharge at intermediate pressures was systematically explored by CCD camera imaging of light-emission fluctuations from the discharge. It was found that column head oscillations inject a high-frequency ionization wave into the positive column if a threshold in discharge current is exceeded. The high-frequency wave decays along the discharge axis towards the anode. Simultaneously, the eigenmode of the positive column increases in amplitude towards the anode. Regular spatiotemporal dynamics occurs when both waves were commensurate. Incommensurate waves lead to different stages of spatiotemporal complexity. Spatiotemporal complexity could be measured and the results were employed for the characterization of the films. Regular dynamics, defect turbulence, weak space-time chaos, and intermittence were found. The wave dynamics was revealed by the biorthogonal decomposition of the space-time data. For irregular waves the mechanism of high-frequency wave decay in the positive column is influenced by transiently occurring wave modes.

Our results give an explanation of the complex dynamics described earlier [20]. Open questions arising from our investigations are the explanation of the mechanism of column head oscillations. More detailed analysis of the transitions from regular windows to developed irregularity seems to be a very promising subject in the context of research on intermittence.

Both the variety of different plasma states and a comparably uncomplicated experimental approach make the discharge an interesting model system for the examination of complex spatiotemporal dynamics.

ACKNOWLEDGMENTS

This work was funded by the Deutsche Forschungsgemeinschaft through Sonderforschungsbereich 198 Kinetik partiell ionisierter Plasmen. The authors are indebted to Dr. Bernd Pompe who provided the estimation of the Kolmogorov entropy.

[1] M. C. Cross and P. C. Hohenberg, Rev. Mod. Phys. **65**, 851 (1993).
[2] K. G. Müller, Phys. Rev. A **37**, 483 (1988).
[3] Ji-Bin Du, Chi-Hui Chiang, and Lin I, Phys. Rev. E **54**, 1829 (1996); Chih-Yi Liu and Lin I, *ibid.* **57**, 3379 (1998).
[4] E. Ammelt, Yu. A. Astrov, and H.-G. Purwins, Phys. Rev. E **58**, 7109 (1998).
[5] Yu. P. Raizer, *Gas Discharge Physics* (Springer, Berlin, 1991).
[6] A. V. Nedospasov, Usp. Fiz. Nauk **94**, 439 (1968) [Sov. Phys. Usp. **11**, 174 (1968)]; L. Pekarek, *ibid.* **94**, 463 (1968) [**11**, 188 (1968)]; R. N. Franklin, *Plasma Phenomena in Gas Discharges*, The Oxford Engineering Science Series (Clarendon, Oxford, 1976).
[7] B.-P. Koch, B. Bruhn, and N. Goepp, Phys. Rev. E **56**, 2118 (1997).
[8] M. Novak, Czech. J. Phys., Sect. B **10**, 954 (1960).
[9] S. Pfau and A. Rutscher, Beitr. Plasmaphys. **4**, 11 (1969) (in German).
[10] W. Pupp, Phys. Z. **33**, 844 (1932).
[11] A. Dinklage, B. Bruhn, H. Deutsch, P. Jonas, B.-P. Koch, and C. Wilke, Phys. Plasmas **5**, 833 (1998).
[12] Rare gas discharges particularly consists of a considerable amount of atoms in metastable states (which will be referred as *metastable atoms*. These metastable atoms play an important role for the formation of ionization waves through stepwise ionization processes.
[13] H. Achterberg and J. Michel, Ann. Phys. (Leipzig) **2**, 365 (1959).
[14] A. Garscadden, *Ionization Waves in Glow Discharges* in *Gaseous Electronics*, edited by M. N. Hirsh and H. J. Oskam (Academic, New York, 1978), Vol. 1.
[15] L. Sirghi, K. Ohe, and G. Popa, J. Phys. D **31**, 551 (1998).
[16] N. L. Oleson and A. W. Cooper, Adv. Electron. Electron. Phys. **24**, 155 (1968); P. S. Landa, N. A. Miskinova, and Yu. V. Ponomarev, Usp. Fiz. Nauk **132**, 601 (1980) [Sov. Phys. Usp. **23**, 813 (1980)].
[17] B. Bruhn, B.-P. Koch, and N. Goepp, Physica D **115**, 353 (1998); B. Bruhn, B.-P. Koch, and P. Jonas, Phys. Rev. E **58**, 3793 (1998); M. Rottmann and K.-H. Spatschek, J. Plasma Phys. **60**, 215 (1998); P. Jonas, B. Bruhn, B.-P. Koch, and A. Dinklage, Phys. Plasmas **7**, 729 (2000).
[18] M. J. Druyvestein and F. M. Penning, Rev. Mod. Phys. **12**, 87 (1940); A. Dinklage, M. Otte, S. Pfau, and C. Wilke, *Proceedings of 1998 ICPP and 25th EPS Conference on Contr. Fusion and Plasma Physics*, edited by P. Pavlo (European Physical Society, Praha, 1998); Europhys. Conf. Abstr. **22C**, 2453 (1998).
[19] K. Wojaczek and A. Rutscher, Beitr. Plasmaphys. **3**, 217 (1963) (in German).
[20] J. R. M. Coulter, J. Electron. Control **9**, 41 (1960); R. S. Stewart, W. F. May, K. G. Emeleus, R. J. M. Coulter, and N. H. K. Armstrong, Int. J. Electron. **18**, 65 (1964).
[21] W. F. May, M.Sc. thesis, The Queen's University, Belfast, 1964 (unpublished).
[22] P. J. Holmes, J. L. Lumley, G. Berkooz, J. C. Mattingly, and R. W. Wittenberg, Phys. Rep. **287**, 337 (1997).
[23] W. Kaufmann, Ann. Phys. (Leipzig) **2**, 158 (1900) (in German).
[24] The programs applied for estimation of correlation dimension and Lyapunov exponents can be found at http://www.mpipks-dresden.mpg.de/~tisean/TISEAN_2.0/index.html; a description of the software is given in R. Hegger, H. Kantz, and T. Schreiber, Chaos **9**, 413 (1999).
[25] D. Prichard and J. Theiler, Physica D **84**, 476 (1995); B. Pompe, *A Tool to Measure Dependencies in Data Sequences* in *Advanced Mathematical Tools in Metrology II*, edited by P. Ciarlini, M. G. Cox, F. Pavese, and D. Richter (World Scientific, Singapore, 1996), p. 81.
[26] A. S. Mikhailov and A. Y. Loskutov, *Foundations of Synergetics Vol. II*, 2nd ed. (Springer-Verlag, Berlin, 1996).
[27] M. Meixner, S. C. Zoldi, S. Bose, and E. Schöll, Phys. Rev. E **61**, 1382 (2000).
[28] P. Beyer, S. Benkadda, and X. Garbet, Phys. Rev. E **61**, 813 (2000).
[29] T. Dudok de Wit, A. L. Pecquet, J. C. Vallet, and R. Lima, Phys. Plasmas **1**, 3288 (1994).
[30] H. Chaté, in *Disordered Regimes of the One-Dimensional Complex Ginzburg-Landau Equation Spatio-Temporal Patterns*, edited by P. E. Gladis and P. Palffy-Muhoray (Addison-Wesley, Reading, MA, 1995), p. 33.